Analysis of atmospheric thermodynamics using the R package aiRthermo

Jon Sáenz[a,b,*], Santos J. González-Rojí[a,c,d], Sheila Carreno-Madinabeitia[e,a], Gabriel Ibarra-Berastegi[f,b]

[a] *Dept. Applied Physics II, Universidad Del País Vasco-Euskal Herriko Unibertsitatea (UPV/EHU), Barrio Sarriena s/n, 48940, Leioa, Spain*
[b] *BEGIK Joint Unit IEO-UPV/EHU, Plentziako Itsas Estazioa (PIE, UPV/EHU), Areatza Pasealekua, 48620, Plentzia, Spain*
[c] *Oeschger Centre for Climate Change Research, University of Bern, Bern, Switzerland*
[d] *Climate and Environmental Physics, University of Bern, Bern, Switzerland*
[e] *Meteorology Area, Energy and Environment Division, TECNALIA R&I, Basque Country, Spain*
[f] *Dept. Nuc. Eng. and Fluid Mech., Universidad Del País Vasco-Euskal Herriko Unibertsitatea (UPV/EHU), Alameda Urquijo S/n, 48013, Bilbao, Spain*

ARTICLE INFO

ABSTRACT

The publicly available R package *aiRthermo* is presented in this study, which allows the user to process information relative to atmospheric thermodynamics, ranging from calculating the density of dry or moist air and converting data between moisture indices to processing a full sounding, obtaining factors such as the convective available potential energy, additional instability indices, or adiabatic evolutions of particles. The package also provides the possibility to present information using customisable Stüve diagrams. Many of the functions are written inside a C extension to ensure that the computations are fast. The results of applying this package to five years of real soundings measured over the Iberian Peninsula are also presented as an example. The package considerably extends the capabilities of R to process atmospheric soundings or model results. This will be useful for many practical environmental forecasting applications at different scales, such as statistical downscaling for climate analysis, quantitative precipitation forecasting (particularly precipitation extremes), diagnosing storms, flash floods, and lightning, and in aviation and other fields where computing atmospheric convection and its related parameters is important.

1. Introduction

R (https://www.cran.r-project.org/) is a freely available software for statistical computing that has expanded exponentially in recent years. Some packages at the intersection between air pollution, climate, and atmospheric studies make R a powerful tool for processing data and visualising atmospheric processes, such as air pollution (Carslaw and Ropkins, 2012) and hydrology (Serrano-Notivoli et al., 2017), and mapping (Skøien et al., 2014) processing satellite (Busetto and Ranghetti, 2016) and atmospheric data (Bowman and Lees, 2015). Additional useful packages in this field, such as *RAtmosphere*, *ClimDown*, *opentraj*, and others, can be downloaded from the Comprehensive R Archive Network (CRAN) repository.

However, the analysis of atmospheric soundings and water vapour from the perspective of atmospheric thermodynamics is an area where the community of atmospheric scientists have new needs using R, as identified by the authors. *aiRthermo* extends the functionality offered by the *RadioSonde* and *meteogRam* packages by adding Stüve diagrams and the vertical evolution of air parcels.

Under the typical pressure and temperature conditions found in the atmosphere, the state of dry air is commonly described by two thermodynamic variables (pressure P and temperature T). The concentration of water can be expressed using different moisture indices, such as the specific humidity, mixing ratio, virtual temperature, and relative humidity. Phase changes of water cause large latent heat fluxes that must be considered as air parcels ascend or descend (Bohren and Albrecht, 1998; Petty, 2008; North and Erukhimova, 2009) when studying atmospheric stability and convection.

Some instability indices are often used when diagnosing meteorological situations. For example, the relationship between sea breeze and precipitation over Hainan Island (Liang and Wang, 2017), the role of moist convection in the development of flash floods (Doswell et al., 1996), or the retrieval of precipitation in the Tropical Rainfall Measuring Mission (TRMM) mission (Petković and Kummerow, 2017), to

name a few. Thermodynamic variables and indices are also used for the statistical downscaling of extreme precipitation events and moisture transport (Ibarra-Berastegi et al., 2011).

The main objective of this paper is to present an R package that has been designed to allow scientists to conduct computations involving atmospheric thermodynamics using the R language. This considerably extends the capabilities of R for meteorological data analysis, and has, for instance, allowed us to extend the lectures offered at the M.Sc. level (Sáenz et al., 2018a), enabling students to perform numerical exercises involving with these parameters.

2. Data

2.1. Sample data provided with the package

The data used in Section 4 of this paper (provided in the package for testing by users) were collected from a server located at the University of Wyoming (publicly available at http://weather.uwyo.edu/upperair/sounding.html). The first sounding used in this paper (sounding A) was measured at Santander, Spain (station ID 08023, date 2010-06-16, 12:00 UTC), and corresponds to a day that faced some frontal rain. The second case (sounding D) was measured at Barcelona, Spain (station ID 08190, 2013-08-07, 12:00 UTC) and reflects a situation with substantial convective instability. The final example (Davenport, USA, station ID 74455, 1997-06-21 at 00 UTC) is also used to illustrate a case with strong convection (Tsonis, 2002).

2.2. Data for the case study

The topography of the Iberian Peninsula and the positions of the eight sounding sites are shown in Fig. 1. The sounding files downloaded from Wyoming University's server covered the period of 2010–2014. The number of cases depends on the site, and ranges from 1705 over Lisbon to 3575 over Murcia. The instability index values computed at Wyoming University and those computed using the functions in aiR-thermo were compared. In aiRthermo, the initial conditions for CAPE were obtained by vertically averaging the lowest 500 m of the sounding and by performing isobaric precooling for the resulting low-level average particle values.

3. Methodology

Most of the theory and methods used to develop aiRthermo can be found in standard references (Bohren and Albrecht, 1998; Petty, 2008; North and Erukhimova, 2009; Tsonis, 2002; Rogers and Yau, 1989).
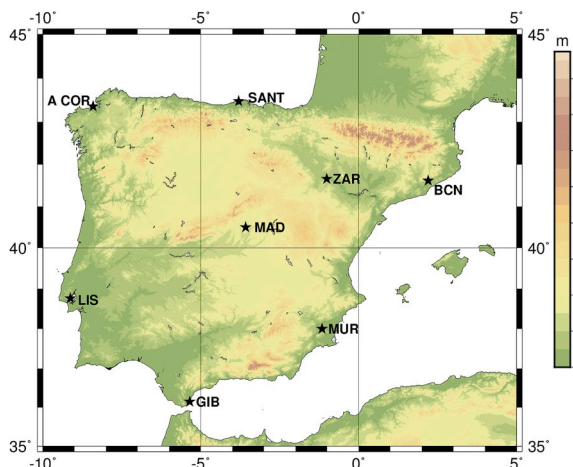

Fig. 1. Map of the Iberian Peninsula showing the stations where soundings are routinely measured.
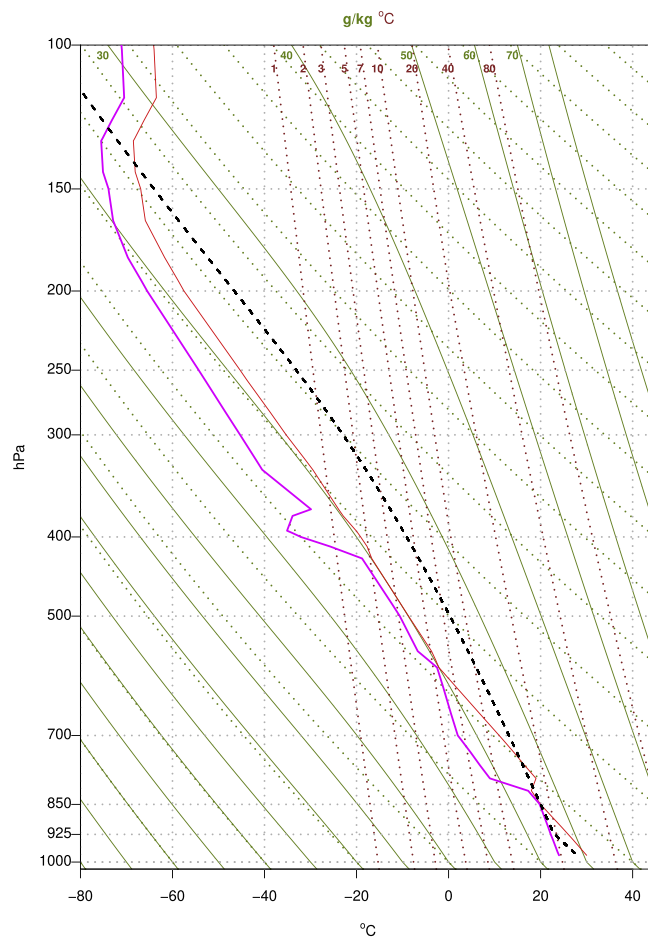

Fig. 2. Example of a Stüve diagram plotted with aiRthermo. The temperature (red) and dew point temperature (magenta) of the sounding area are plotted together with the evolution of the lifted air parcel (dashed black line). (For interpretation of the references to colour in this figure legend, the reader is referred to the Web version of this article.)

However, some of our assumptions are documented below.

The state of an air parcel is defined in aiRthermo using its pressure P (Pa), temperature T (K), and mixing ratio w (kg kg^{-1}). To compute the saturation pressure of water over a flat surface, we follow the expressions on pages 197–200 from (Bohren and Albrecht, 1998) for ice and water below 30 °C, and Buck's equation (Buck, 1981) above 30 °C. The dew-point temperature is given by the approximate expression of 5.68 in (Bohren and Albrecht, 1998) from the given P and mixing ratio w.

The specific heat of moist air at a constant pressure and volume are computed as $c_{pm} = c_{pd}(1 + 0.87q)$ and $c_{vm} = c_{vd}(1 + 0.97q)$, following (Tsonis, 2002), with $c_{pd} = 1005$ J kg^{-1} K^{-1} and $c_{vd} = 718$ J kg^{-1} K^{-1} (Bohren and Albrecht, 1998; Petty, 2008). By default, the functions that provide these specific heats will return the values corresponding to moist air, and values corresponding to dry air can be requested by explicitly building a dry air parcel.

A good analytical expression for the latent heat of evaporation of water does not exist, therefore, an approximate expression is used. For liquid water ($T \in [233.15, 313.15]$ K interval), we use cubic polynomial expansion based on tabulated values (Rogers and Yau, 1989) with an absolute residual smaller than 1 J kg^{-1}, and all terms are statistically significant at the 99% confidence level. By doing this, we assume that super-cooled water can exist up to the Schaefer point (about −40 °C). The result for ice is based on a quadratic fit to the observed values (Feistel and Wagner, 2006) in the interval of $T \in [210,273.15]$ K (residuals smaller than 0.05 J kg^{-1}). As the values corresponding to water and ice differ in the common interval used in the previous two

expressions, a linear combination of ice's (L_i) and water's (L_w) latent heat is computed $L = w_i L_i + (1 - w_i) L_w$ with a weight of $w_i = 1 - \frac{T - 253.15}{20}$ in the interval of $T \in [253.15, 273.15]$ K. Below 253.15 K, the latent heat corresponding to ice is applied, and that corresponding to water is used above 273.15 K.

All vertical evolutions are computed assuming that hydrostatic balance is in place. Therefore, $\Gamma_d^* = \left(\frac{dT}{dP}\right)_d = \frac{\Gamma_d}{\rho g}$ and $\Gamma_s^* = \frac{\Gamma_s}{\rho g}$ are used, with Γ_d and Γ_s as the typical expression for vertical gradients in Z. For the saturated pseudoadiabatic profile, the expression used for the pressure coordinates is transformed from the common expression provided in z (Bohren and Albrecht, 1998; Petty, 2008; North and Erukhimova, 2009; Tsonis, 2002). Using the expressions of Γ_d^* (Γ_s^*) for dry (saturated) adiabatic evolutions, the vertical evolution of an air parcel from the initial state P_0, T_0, and w_0 is computed by numerically solving the ordinary differential equation $\frac{dT}{dP} = \Gamma_i^*(P, T, w)$, with $i = d$ or $i = s$ depending whether or not the particle is saturated. This differential equation is numerically solved using the fourth-order Runge-Kutta scheme for all vertical evolutions, with saturation checks at each vertical step.

For some of the indices, such as the Lifted Index (LI) or Convective Available Potential Energy (CAPE), it is customary to calculate the vertical average of the lower levels to identify a representative parcel P_0, T_0, w_0 of the lowest levels of the atmosphere (Craven et al., 2002; Letkewicz and Parker, 2010). These vertical averages at low levels are evaluated in all cases by first considering

$$\Delta Z = \frac{R_d}{g} \int_{P_t}^{P_s} \frac{T_v dP}{P} \tag{1}$$

as the vertical width of the parcel. Next, the accumulated vertical quantity value $X(P)$ is given by

$$\bar{X} = \frac{1}{\Delta Z} \frac{R_d}{g} \int_{P_t}^{P_s} \frac{X k T_v}{P} dP \tag{2}$$

where $k(P)$ serves as a normalising function. When calculating the average temperature, $k(P) = 1$ is used. In contrast, the specific humidity $k(P) = q(P)$ is used to indicate moisture. The vertical integrals are computed using discrete slabs defined by the data given by the soundings in all cases. For these discrete slabs, the integrals are computed analytically and the results are accumulated.

To compute CAPE and convective inhibition (CIN), the vertical integrals are computed in pressure levels by adding the energy corresponding to discrete slabs defined by linear or logarithmic vertical profiles, which are defined by the soundings. The integrals for each of the slabs enclosed by linear profiles are computed analytically, and the energy corresponding to each slab is accumulated, producing the final value of CAPE or CIN. The integrals are always calculated using the virtual temperature (Doswell and Rasmussen, 1994).

There are different methods of accurately determining the lifting condensation level (LCL) or the equivalent potential temperature of an air parcel in *aiRthermo*. In the first case, the package calculates these variables by computing their vertical evolutions and numerically solving the ordinary differential equation representing their ascent from the initial conditions given by their temperature, pressure, and mixing ratio. For compatibility, functions that allow these variables from well-known alternative equations to be computed, such as the approximate method presented by Bolton (1980) to compute LCL, are also provided.

The routine designed to produce Stüve diagrams for either the soundings or the lifted particles used in the computation of CAPE/CIN extends the available options for thermodynamic diagrams in the existing *RadioSonde* R package. The routine that plots the Stüve diagram uses the equivalent potential temperature lines, constant mixing ratio lines, or dry adiabatic lines produced by the routines in *aiRthermo* to ensure the full consistency of results. The routine that plots the Stüve diagram allows the user to plot additional lines in the sounding, enabling the production of highly customisable plots.

4. Description of the package

The package contains over 40 functions that can be separated into six large groups according to their functionality. A brief description of each set of functions is presented here, however, the manual of the package must be checked for a full description of the functions and the parameters required to run them. The manual can be found on the webpage for the package *aiRthermo* in CRAN.

- Density of dry/moist air and virtual temperature

The density of air can be directly calculated using the corresponding function densityMoistAir, or by using intermediate functions to independently calculate the densities of dry air and water vapour (densityDry and densityH2Ov). The virtual temperature of an air parcel can also be directly calculated by using the virtual_temperature function.

- Conversion of moisture indices

Several functions that allow conversion between moisture indices through the dew point temperature, mixing ratio, and specific or relative humidity are included in *aiRthermo*. The most important functions of this category are those converting the relative humidity to the mixing ratio (rh2w), the relative humidity to the specific humidity (rh2shum), the mixing ratio to the dew point temperature (w2Td), and the mixing ratio to the specific humidity or the reverse (w2q and q2w), or e2w to convert the partial pressure of water vapour to the mixing ratio.

- Saturation mixing ratios or pressures

This class includes all functions that use the Clausius-Clapeyron equation to calculate the saturation mixing ratios or pressures. The most important function is saturation_pressure_H2O, which computes the saturation pressure e_s in Pa as a function of the temperature. As well as this, saturation_mixing_ratio returns the saturation mixing ratio w_s in kg kg^{-1}.

- State and evolution of an air parcel

The package calculates the internal state of a parcel using a given pressure, temperature, and mixing ratio with the function parcelState. However, to calculate the vertical evolution of an air parcel, *aiRthermo* determines the correct function depending on the state of the particle and the environment. General ascent from a given initial pressure to the final pressure is computed by the adiabatic_ascent function, which selects the type of evolution depending on the saturation of the parcel. Downwards evolution can also be computed using AnyAdiabaticDown, but it requires the initial amount of water available in the cloud for evaporation (in kg/kg). Conversions between the potential temperature, temperature, and pressure can be calculated using PT2Theta, PTheta2T, and TTheta2P, which are useful if dry adiabatic processes are occurring.

- Instability indices

Several functions compute common instability indices such as K, the Total-Totals, the Showalter, and the LI indices (functions Kindex, TTindex, Sindex, and LIindex). CAPE_CIN calculates the values of CAPE and CIN, the LCL, the Level of Free Convection (LFC), the End Level (EL), and the trajectory followed by the lifted parcel. The *PlowTop* argument provides the width of a slab across which a vertical average will be taken through the bottom of the sounding to obtain the initial conditions of the ascending parcel. *precoolType* determines the type of precooling that must be applied to the initial parcel. *upToTop* controls
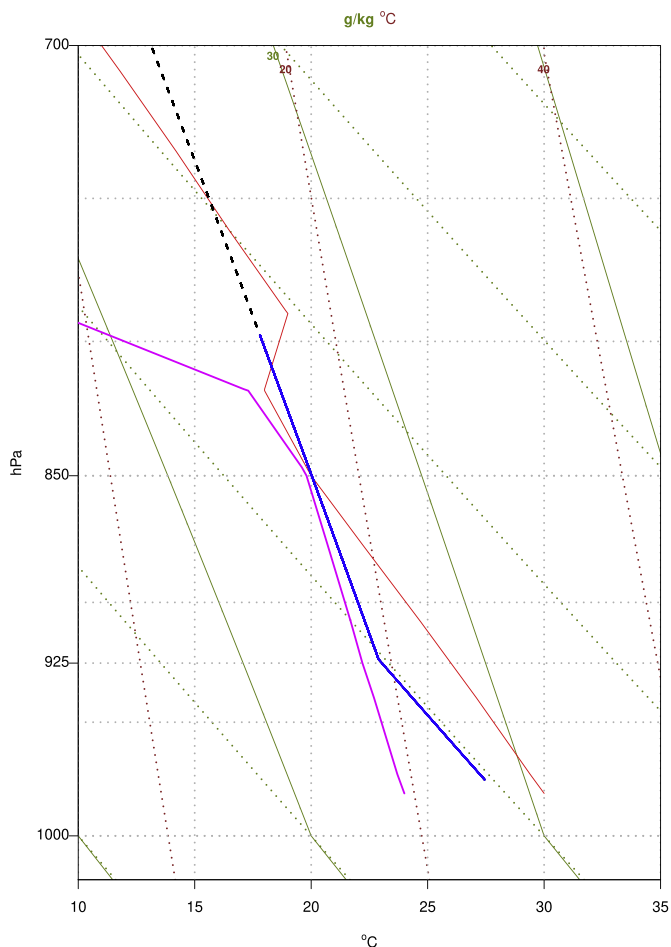
Fig. 3. Detail of the example Stüve diagram in Fig. 2 magnifying its lower levels to show the different evolutions of the lifted parcel depending on the value of the *upToTop* parameter (*TRUE* -black line- and *FALSE* -blue line-). (For interpretation of the references to colour in this figure legend, the reader is referred to the Web version of this article.)

whether the lifted particle continues upwards after it first crosses the ambient sounding.

- Stüve diagrams

The stuve_diagram function is included to allow the creation of high-quality Stüve diagrams. As well as generating the Stüve diagram, they can also represent the trajectory followed by any ascending air parcel (when CAPE_CIN is called using *getLiftedBack = TRUE*).

Fig. 2 shows the Stüve diagram corresponding to the Davenport sample sounding. Major differences in the estimated CAPE for the sounding can appear if the *upToTop* attribute is set to *TRUE* or *FALSE* (discontinuous black and blue lines in Fig. 3 respectively) as the lifting particle slightly crosses the sounding at low levels. These results can be controlled using the appropriate parameters. Sensible default parameters are used by the function if they are not explicitly provided by the user.

Listing 1 shows the manner in which CAPE_CIN can be used to produce a figure similar to Fig. 2. Each time CAPE_CIN is called, *getLiftedBack* can be set to *TRUE* so that the trajectory of the lifted parcel is returned to the calling environment. The dashed black line in Fig. 2 shows the trajectory of the ascending parcel when it is requested to ascend to the top of the sounding (*upToTop = TRUE*). If *FALSE* is assigned to the *upToTop* parameter, the parcel (blue line in Fig. 3) stops after the first time that the ascending parcel is not buoyant, thus leading

to a severe underestimation of the value of CAPE. The buoyancy is evaluated using virtual temperatures for the parcel and the environment in all cases.

Listing 1. Evaluation of CAPE (CIN) and a representation of a sounding.

```
data(RadiosondeDavenport)
dPs<-RadiosondeDavenport[,1]*100
dTs<-C2K(RadiosondeDavenport[,3])
dws<-RadiosondeDavenport[,6]/1000
# Dew point T in Celsius for plotting
dTd<-RadiosondeDavenport[,4]
# Initial conditions are known.
# upToTop<-FALSE "stop after the parcel is not buoyant"
capeOut<-CAPE_CIN(Ps=dPs,Ts=dTs,ws=dws,deltaP=1,
        P0=97500,T0=300.6,w0=0.01936,upToTop=FALSE,
        getLiftedBack=FALSE,precoolType="none")
# some of the information from the output object
print(paste("Davenport_CAPE:",capeOut$cape,
        "J/kg","CIN:",capeOut$cin,"J/kg","LFC",
        capeOut$apLFC$P,"Pa",capeOut$apLFC$Temp,"K"))
# Whole sounding (upToTop<-TRUE), parcel is returned
capeOut<-CAPE_CIN(Ps=dPs,Ts=dTs,ws=dws,deltaP=1,
        P0=97500,T0=300.6,w0=0.01936,
        upToTop=TRUE,getLiftedBack=TRUE)
# Plot sounding
plot<-stuve_diagram(Pres=dPs/100,Temp=K2C(dTs))
# Dew point temperature
lines(dTd,dPs/100,col="magenta",lwd=2)
# Lifted parcel (upToTop=TRUE)
lines(K2C(capeOut$Tl),(capeOut$Pl/100),
        col="black",lwd=2,lty=2)
```

A profiler has been used to evaluate the CPU time that *aiRthermo* requires to calculate saturated adiabatic evolution from an initial pressure of 950 hPa to 200 hPa (pressure step of 1 Pa). A routine that performs the same computation using an R iteration was also written. The evolution takes 50 ms using *aiRthermo*, however, that using R alone takes approximately 1500 ms. Therefore, the speed is approximately thirty times faster due to the use of the C core for computing vertical evolutions.

5. Case study: instability indices over the Iberian Peninsula (2010–2014)

The performance of the package has been checked using a large number of real soundings measured over the Iberian Peninsula (Fig. 1), an area well known for the development of convective systems (Viceto et al., 2017).

In this case study, 24072 soundings from the eight stations were processed to estimate the performance of the package using realistic data. CAPE and CIN were computed using a very low vertical step (0.5 Pa), and all the soundings extended to the top of the sounding. CAPE and CIN were computed twice for two different initial parcels (one from the lowest point of the sounding, and the second from a low-level average). The K, Total-Totals, Lifted, and Showalter indices were also computed. This process took 6 h on a common desktop computer (2015) running Linux.
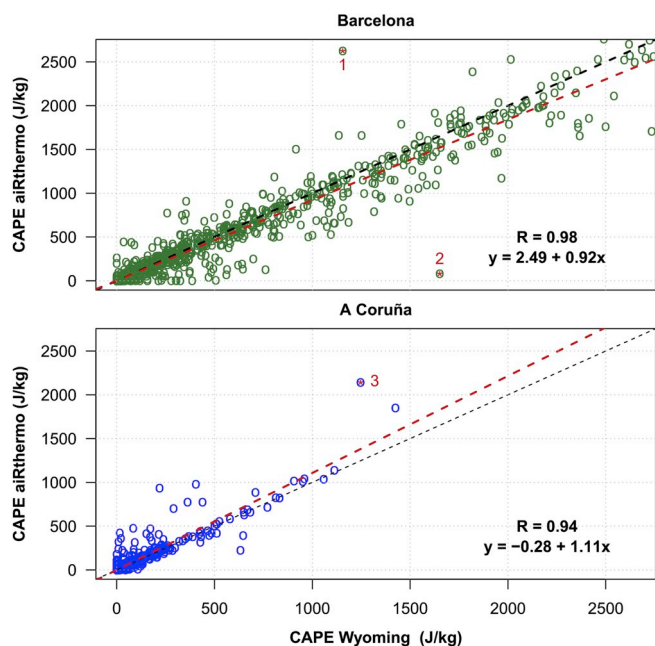
Fig. 4. Scatterplot of the CAPE values computed by *aiRthermo* and the corresponding values computed by the University of Wyoming for Barcelona (top) and A Coruña (bottom).

The results of CAPE computed by *aiRthermo* and the value stored at the University of Wyoming server were compared. Fig. 4 shows the resulting scatterplots for A Coruña (Atlantic site) and Barcelona (Mediterranean). The Pearson's correlation coefficient R value is very good in both cases, at 0.94 in A Coruña (3521 soundings) and 0.98 in Barcelona (3575 soundings). The values of R were within a range of [0.94, 0.99] at all stations.

As shown in Fig. 4, there are some clear outliers in the scatterplots. An analysis comparing some of these points (tagged with numbers) that yield different CAPE values to those provided by Wyoming has been conducted. In the first case (Barcelona, May 8th, 2011), *aiRthermo* computes a CAPE of 2625 J/kg, while Wyoming computes a CAPE of 1155 J/kg. This difference is due to the sensitivity to the initial conditions that characterise the CAPE value. We cannot be certain of the manner in which the vertical evolutions are initialised in the Wyoming server, but we have verified that errors smaller than 2% in the estimation of the initial state of the parcel (its pressure or temperature) lead to differences of 100% between the resulting CAPE values of this sounding, characterised by almost complete saturation until 500 hPa. The second case (Barcelona, August 26th, 2012) corresponds to a sounding with no moisture in the mixing ratio column of the Wyoming archive beyond 700 hPa. As the data are missing, aiRthermo is forced to stop at that level because there is no moisture information in the mixing ratio column. If the mixing ratio is assumed to be zero beyond that point and the whole sounding is processed, the differences are small (1767 J/kg in *aiRthermo* vs 1651 J/kg in Wyoming). Finally, the third analysed example corresponds to A Coruña, 27th June 2012. In this case, the mixing ratio column in the table distributed by Wyoming contains zeros. However, the moisture is not completely missing. A value of CAPE similar to that on Wyoming's web page (1247 J/kg) is computed by *aiRthermo* (1211 J/kg) if the moisture is computed from the dew point temperature in Wyoming's server.

Although the exact initial conditions used for computing CAPE in Wyoming are unknown to us, which means that the sensitivity of the results caused by this cannot be fully evaluated, the least squares regression lines exhibit high agreement, with slopes very close to one (0.92 and 1.11, as shown in Fig. 4).

6. Discussion and conclusions

This paper presents a new package for R, *aiRthermo*, which is available in the open-source repository for R packages CRAN. It provides R with new functions in the field of atmospheric thermodynamics. These capabilities considerably extend the analyses that can be conducted from inside the R interpreter.

In the field of storm forecasting, the parameters that can be computed using *aiRthermo* have been used to forecast storms in Belgrado (Vujović et al., 2015). Therefore, the ability to run different statistical models and verification procedures from inside R alongside computing the indices themselves could boost this type of study. Similar analysis (Czernecki et al., 2015) has been conducted in the Arctic region (Bjørnøya, Jan Mayen and Svalbard Islands), and the results of the distribution of instability indices were very different to those of other European regions (Siedlecki, 2009). The instability indices available in *aiRthermo* have been combined with satellite data from regional instability indices in Africa (de Coning et al., 2011) and India (Chaudhuri et al., 2013). These results show that analysing the climatological distribution of atmospheric instability (Siedlecki, 2009), its interannual variability, and its expected future distribution (Viceto et al., 2017) under globally changing conditions can benefit from using *aiRthermo*. As some instability indices must be computed from vertical adiabatic evolutions of air parcels close to the surface (the case of CAPE or LI), analysing these distributions is easier if every sounding can be processed in a much shorter time (as performed by *aiRthermo*). This will increase the use of instability indices in downscaling methods that are designed to operate on daily precipitation (Iizumi et al., 2011), even for long periods of time.

As well as precipitation forecasts, other damaging effects can be derived from atmospheric convective instability. Atmospheric instability indices are used to analyse lightning in Western Patagonia (Garreaud et al., 2014) and the Iberian Peninsula (Santos et al., 2013). They also serve as prognostic variables when statistically downscaling wind variability (Davy et al., 2010). The aircraft safety field is another area where the thermodynamic properties of air, particularly when it is close to saturation, are important, both at the surface, during the prevention of fog (when studying ice fog, for example (Gultepe et al., 2015)), or aloft to prevent the aircraft from icing (Bernstein et al., 2007).

The authors have also recently used the package for educational purposes in the case of M.Sc. studies in the University of the Basque Country (Sánchez-Lavega et al., 2014). Students use the routines in the package to numerically simulate the vertical evolution of parcels and verifying their results with those they obtain from thermodynamic diagrams. They also assess the role of large-scale moisture convergence against convection in intense precipitation events by computing instability indices for air parcels, and solve simple exercises related to the Föhn effect (Sáenz et al., 2018a).

There is a perpetual need for verifying complex forecasting systems based on advanced numerical models. The diagnostics available in *aiRthermo* are often used in these verification processes (Jones et al., 2017). The direct availability of these diagnostics from the package used for the verification (frequently R itself) will quicken the development of these models. This also includes new satellite systems, such as GOES-R (Schmit et al., 2008, 2009), which can produce integrated instability indices, such as LI, almost in real-time. The ability to easily compute the values of LI, CAPE, or other indices from soundings, satellite sounders (Lee et al., 2016; Schmit et al., 2017), and numerical model results will increase the ease of the interoperability of modelled and observational data (soundings, satellite-derived products, and remotely sensed information) in newly developed operational environmental forecasting systems.

Declarations of interest

The only interest of the authors is to make the package known. If the paper is accepted, their scientific merit will also be publicly recognised.

Authorship statement

Jon Sáenz thought up the original concept of the package, wrote most parts of the C code, several parts of the R code, and some of the verification routines. He was also the lead author of the paper. **Santos J. González-Rojí** wrote some parts of the R and verification codes, packaged the software for its inclusion in CRAN, and wrote some parts of the paper. **Sheila Carreno-Madinabeitia** was the author of the Stüve plotting routines and parts of the verification code. She analysed the sounding database presented in the paper and participated in the writing. **Gabriel-Ibarra Berastegi** was involved in the verification of results, the testing of the package, and the writing of the paper.

Appendix A. Supplementary data

Supplementary data to this article can be found online at https://doi.org/10.1016/j.cageo.2018.10.007.

Software and data availability

The software presented in this paper is a package prepared to work within the R data analysis suite and was developed by the authors:

- Jon Sáenz
- Santos J. González-Rojí.
- Sheila Carreno-Madinabeitia
- Gabriel Ibarra-Berastegi

Contact address: Jon Sáenz, Dept. of Applied Physics II, Faculty of Science and Technology, UPV/EHU, Barrio Sarriena s/n, 48940-Leioa, Spain. Telephone: +34 946012445 Fax: +34 946013500.

Email addresses:

- jon.saenz@ehu.eus
- santosjose.gonzalez@ehu.eus
- sheila.carreno@tecnalia.com
- gabriel.ibarra@ehu.eus

Year first available in CRAN: 2017.

Hardware required: It has been tested on laptops, Desktops, and workstations running Mac OS, Windows, and Linux.

Availability: The software and datasets are freely available (GPL-3 license) in the Comprehensive R Archive Network (CRAN): https://cran.r-project.org/package=aiRthermo.

The package can be installed from any of the mirrors, which is usual for R packages, by typing install.packages("aiRthermo") into the R interpreter. The size of the package ranges from 400 to 500 Kb, depending on whether the source or Windows-compiled version is downloaded. The CRAN servers allow anonymous access to the package. The software is written in R and C. The manual is also provided at the CRAN server (Sáenz et al., 2018b).

References

Bernstein, B.C., Wolff, C.A., McDonough, F., 2007. An inferred climatology of icing conditions aloft, including supercooled large drops. Part I: Canada and the continental United States. J. Appl. Meteorol. Climatol. 46, 1857–1878. https://doi.org/10.1175/2007JAMC1607.1.

Bohren, C.F., Albrecht, B.A., 1998. Atmospheric Thermodynamics. Oxford University Press, New York.

Bolton, D., 1980. The computation of equivalent potential temperature. Mon. Weather Rev. 108, 1046–1053. https://doi.org/10.1175/1520-0493(1980)108<1046:TCOEPT>2.0.CO;2.

Bowman, D., Lees, J., 2015. Near real time weather and ocean model data access with rNOMADS. Comput. Geosci. 78, 88–95. https://doi.org/10.1016/j.cageo.2015.02.013.

Buck, A.L., 1981. New equations for computing vapor pressure and enhancement factor. J. Appl. Meteorol. 20, 1527–1532. https://doi.org/10.1175/1520-0450(1981)020<1527:NEFCVP>2.0.CO;2.

Busetto, L., Ranghetti, L., 2016. MODIStsp: an R package for automatic preprocessing of MODIS Land Products time series. Comput. Geosci. 97, 40–48. https://doi.org/10.1016/j.cageo.2016.08.020.

Carslaw, D.C., Ropkins, K., 2012. Openair an R package for air quality data analysis. Environ. Model. Software 27–28, 52–61. https://doi.org/10.1016/j.envsoft.2011.09.008.

Chaudhuri, S., Pal, J., Middey, A., Goswami, S., 2013. Nowcasting Bordoichila with a composite stability index. Nat. Hazards 66, 591–607. https://doi.org/10.1007/s11069-012-0504-y.

Craven, J.P., Jewell, R.E., Brooks, H.E., 2002. Comparison between observed convective cloud-base heights and lifting condensation level for two different lifted parcels. Weather Forecast. 17, 885–890. https://doi.org/10.1175/1520-0434(2002)017<0885:CBOCCB>2.0.CO;2.

Czernecki, B., Taszarek, M., Kolendowicz, L., Szyga-Pluta, K., 2015. Atmospheric conditions of thunderstorms in the European part of the Arctic derived from sounding and reanalysis data. Atmos. Res. 154, 60–72. https://doi.org/10.1016/j.atmosres.2014.11.001.

Davy, R.J., Woods, M.J., Russell, C.J., Coppin, P.A., 2010. Statistical downscaling of wind variability from meteorological fields. Boundary-Layer Meteorol. 135, 161–175. https://doi.org/10.1007/s10546-009-9462-7.

de Coning, E., Koenig, M., Olivier, J., 2011. The combined instability index: a new very-short range convection forecasting technique for southern Africa. Meteorol. Appl. 18, 421–439. https://doi.org/10.1002/met.234.

Doswell III, C.A., Rasmussen, E.N., 1994. The effect of neglecting the virtual temperature correction on CAPE calculations. Weather Forecast. 9, 625–629. https://doi.org/10.1175/1520-0434(1994)009<0625:TEONTV>2.0.CO;2.

Doswell III, C.A., Brooks, H.E., Maddox, R.A., 1996. Flash flood forecasting: an ingredients-based methodology. Weather Forecast. 11, 560–581. https://doi.org/10.1175/1520-0434(1996)011<0560:FFFAIB>2.0.CO;2.

Feistel, R., Wagner, W., 2006. A new equation of state for H2O ice Ih. J. Phys. Chem. Ref. Data 35, 1021–1047. https://doi.org/10.1063/1.2183324.

Garreaud, R.D., Nicora, M.G., Bürgesser, R.E., Ávila, E.E., 2014. Lightning in western Patagonia. J. Geophys. Res.: Atmosphere 119, 4471–4485. https://doi.org/10.1002/2013JD021160.

Gultepe, I., Zhou, B., Milbrandt, J., Bott, A., Li, Y., Heymsfield, A., Ferrier, B., Ware, R., Pavolonis, M., Kuhn, T., Gurka, J., Liu, P., Cermak, J., 2015. A review on ice fog measurements and modeling. Atmos. Res. 151, 2–19. https://doi.org/10.1016/j.atmosres.2014.04.014.

Ibarra-Berastegi, G., Sáenz, J., Ezcurra, A., Elías, A., Díaz de Argandoña, J., Errasti, I., 2011. Downscaling of surface moisture flux and precipitation in the Ebro Valley (Spain) using analogues and analogues followed by random forests and multiple linear regression. Hydrol. Earth Syst. Sci. 15, 1895–1907. https://doi.org/10.5194/hess-15-1895-2011.

Iizumi, T., Nishimori, M., Dairaku, K., Adachi, S.A., Yokozawa, M., 2011. Evaluation and intercomparison of downscaled daily precipitation indices over Japan in present-day climate: strengths and weaknesses of dynamical and bias correction-type statistical downscaling methods. J. Geophys. Res.: Atmosphere 116 (D1). https://doi.org/10.1029/2010JD014513. D01111.

Jones, T.A., Koch, S., Li, Z., 2017. Assimilating synthetic hyperspectral sounder temperature and humidity retrievals to improve severe weather forecasts. Atmos. Res. 186, 9–25. https://doi.org/10.1016/j.atmosres.2016.11.004.

Lee, S.J., Ahn, M.-H., Lee, Y., 2016. Application of an artificial neural network for a direct estimation of atmospheric instability from a next-generation imager. Adv. Atmos. Sci. 33, 221–232. https://doi.org/10.1007/s00376-015-5084-9.

Letkewicz, C.E., Parker, M.D., 2010. Forecasting the maintenance of mesoscale convective systems crossing the Appalachian Mountains. Weather Forecast. 25, 1179–1195. https://doi.org/10.1175/2010WAF2222379.1.

Liang, Z., Wang, D., 2017. Sea breeze and precipitation over Hainan Island. Q. J. R. Meteorol. Soc. 143, 137–151. https://doi.org/10.1002/qj.2952.

North, G.R., Erukhimova, T.L., 2009. Atmospheric Thermodynamics. Cambridge University Press, New York.

Petković, V., Kummerow, C.D., 2017. Understanding the sources of satellite passive microwave rainfall retrieval systematic errors over land. J. Appl. Meteorol. Climatol. 56, 597–614. https://doi.org/10.1175/JAMC-D-16-0174.1.

Petty, G.W., 2008. A First Course in Atmospheric Thermodynamics. Sundog Publishing, Madison.

Rogers, R.R., Yau, M.K., 1989. A Short Course in Cloud Physics, third ed. Pergamon Press, Oxford.

Sáenz, J., González-Rojí, S., Carreno-Madinabeitia, S., Ibarra-Berastegi, G., 2018a. Airthermo: an R package designed to help students understanding atmospheric thermodynamics. In: EDULEARN18 Proceedings, 10th International Conference on Education and New Learning Technologies. IATED, pp. 1567–1573.

Sáenz, J., González-Rojí, S.J., Carreno-Madinabeitia, S., Ibarra-Berastegi, G., 2018b. aiRthermo: Atmospheric Thermodynamics and Visualization, R Package Version 1.2. https://CRAN.R-project.org/package=aiRthermo.

Sánchez-Lavega, A., Pérez-Hoyos, S., Hueso, R., del Río-Gaztelurrutia, T., Oleaga, A., 2014. The Aula EspaZio Gela and the Master of Space Science and Technology in the Universidad del País Vasco (University of the Basque Country). Eur. J. Eng. Educ. 39, 518–526. https://doi.org/10.1080/03043797.2013.788611.

Santos, J.A., Reis, M.A., De Pablo, F., Rivas-Soriano, L., Leite, S.M., 2013. Forcing factors of cloud-to-ground lightning over Iberia: regional-scale assessments. Nat. Hazards Earth Syst. Sci. 13 (7), 1745–1758. https://doi.org/10.5194/nhess-13-1745-2013.

Schmit, T.J., Li, J., Li, J., Feltz, W.F., Gurka, J.J., Goldberg, M.D., Schrab, K.J., 2008. The GOES-R advanced baseline imager and the continuation of current sounder products. J. Appl. Meteorol. Climatol. 47, 2696–2711. https://doi.org/10.1175/2008JAMC1858.1.

Schmit, T.J., Li, J., Ackerman, S.A., Gurka, J.J., 2009. High-spectral- and high-temporal- resolution infrared measurements from geostationary orbit. J. Atmos. Ocean. Technol. 26, 2273–2292. https://doi.org/10.1175/2009JTECHA1248.1.

Schmit, T.J., Griffith, P., Gunshor, M.M., Daniels, J.M., Goodman, S.J., Lebair, W.J., 2017. A closer look at the ABI on the GOES-R series. Bull. Am. Meteorol. Soc. 98, 681–698. https://doi.org/10.1175/BAMS-D-15-00230.1.

Serrano-Notivoli, R., de Luis, M., Beguería, S., 2017. An R package for daily precipitation climate series reconstruction. Environ. Model. Software 89, 190–195. https://doi.org/10.1016/j.envsoft.2016.11.005.

Siedlecki, M., 2009. Selected instability indices in Europe. Theor. Appl. Climatol. 96, 85–94. https://doi.org/10.1007/s00704-008-0034-4.

Skøien, J., Blöschl, G., Laaha, G., Pebesma, E., Parajka, J., Viglione, A., 2014. rtop: an R package for interpolation of data with a variable spatial support, with an example from river networks. Comput. Geosci. 67, 180–190. https://doi.org/10.1016/j.cageo.2014.02.009.

Tsonis, A.A., 2002. An Introduction to Atmospheric Thermodynamics. Cambridge University Press, Cambridge.

Viceto, C., Marta-Almeida, M., Rocha, A., 2017. Future climate change of stability indices for the Iberian Peninsula. Int. J. Climatol. 4390–4408. https://doi.org/10.1002/joc.5094. n/a.

Vujović, D., Paskota, M., Todorović, N., Vučković, V., 2015. Evaluation of the stability indices for the thunderstorm forecasting in the region of Belgrade, Serbia. Atmos. Res. 161, 143–152. https://doi.org/10.1016/j.atmosres.2015.04.005.